J. Fluid Mech. (1984), *vol.* 140, *pp.* 135–151
Printed in Great Britain

Unsteady natural convection in a cavity with internal heating and cooling

By JOHN C. PATTERSON

Department of Civil Engineering, The University of Western Australia, Nedlands 6009, Western Australia

(Received 29 December 1982 and in revised form 15 September 1983)

The problem of transient natural convection in a cavity of aspect ratio $A < 1$ driven by internal buoyancy sources and sinks distributed linearly in the horizontal and uniformly in the vertical is considered. Scaling analysis is used to show that a number of possible transient flow regions are possible, collapsing ultimately onto one of conductive, transitional, or convective steady-state flow regimes. A number of numerical solutions are obtained, and their relationships to the scaling analysis are discussed.

1. Introduction

The transport of heat or mass by natural convection is a process that finds frequent application in physical systems, and accordingly has received considerable attention in the literature. In particular, the case of a two-dimensional rectangular cavity with differentially heated endwalls and insulated horizontal boundaries is a particular case that has been studied for several decades.

A class of problem that has received far less attention is that of the motions generated by internal buoyancy fluxes. This class is fundamentally different to the former problem in that the generation mechanism is, at least initially, distributed through the fluid, rather than being concentrated at the boundaries. For the most part, results in this area have been confined to flows in long vertical ducts (e.g. Turcotte, Spence & Bau 1982) or to a modified form of the Bernard problem (e.g. Tritton & Zarraga 1967; Roberts 1967; Thirlby 1970; Kulacki & Goldstein 1972; Kikuchi, Kawasaki & Shioyama 1982). Bergholz (1980) considered the case of a closed cavity with a uniform volumetric heating rate, with the flow being driven by cooling on the sidewalls.

The motivation for some of the recent studies in low-aspect-ratio, differentially heated cavities has been, at least in part, the existence of certain types of geophysical flows (Cormack, Leal & Imberger 1974; Patterson & Imberger 1980), with the differentially heated endwalls corresponding to localized sources and sinks of buoyancy. However, in many cases, a distribution of sources and sinks of buoyancy would provide a better-idealized model of the geophysical situation. Consider, for example, a water body subjected to non-uniform surface cooling due perhaps to a non-uniform wind field. For sufficiently shallow water, the cooling effect may be distributed over the depth, and corresponds to a distribution of buoyancy sinks. The resultant horizontal temperature gradient drives a convective motion which contributes to the horizontal mixing processes; the time and velocity scales of the convective transport in comparison with those of other processes (e.g. vertical mixing, wind-driven circulation) are required to assess this contribution. An idealized model

in this case is then a rectangular cavity containing a distribution of sources and sinks varying horizontally, but not vertically or in time. With insulated boundaries and no vertical variation in source strength, the model becomes a study of the horizontal heat-transfer processes due to the gradient in source strength, in contrast to the modified Bernard problems, which are studies of the vertical heat-transfer mechanism.

Many other distributions could find application in geophysical situations, or perhaps in chemically reacting fluids or heat exchangers, to name two examples. The point of this paper is not, however, directed at the applications, but rather towards an understanding of the processes involved in the convective motions generated by internal, rather than external, buoyancy sources.

In the following, the case of a rectangular two-dimensional cavity of small aspect ratio A containing a fluid of Prandtl number $\sigma > 1$ with a distribution of sources of varying strength is examined. A scaling analysis is used to obtain some insight into the transient behaviour and the development to steady state for a particular, simple source distribution. With the properties of the distribution embodied in the definition of a Grashof number Gr, it is possible to determine a broad classification of flow types, depending on the relative values of Gr, A and σ. The broad classification yields conductive, convective, and transitional regimes, each regime containing a number of subregimes characterized by different approaches to steady state and different steady-state flow and temperature fields. A number of numerical solutions for particular values of Gr, A and σ are obtained with the intention of traversing the principal regimes. The results of the numerical analysis are discussed in the context of the preceding scaling analysis.

2. Formulation and scaling analysis

Under consideration is a closed rectangular two-dimensional cavity of length L and half-height h (aspect ratio $A = h/L$) with rigid, non-slip, thermally insulated boundaries (figure 1). The cavity contains a Newtonian fluid initially at rest and at temperature T_0. At time $t = 0$, a continuous distribution of sources and sinks is enabled and maintained thereafter. The usual Boussinesq equations describe the subsequent flow and temperature fields:

$$\frac{\partial u}{\partial t}+u\frac{\partial u}{\partial x}+v\frac{\partial u}{\partial y}=-\frac{1}{\rho_0}\frac{\partial p}{\partial x}+\nu\nabla^2 u, \tag{1}$$

$$\frac{\partial v}{\partial t}+u\frac{\partial v}{\partial x}+v\frac{\partial v}{\partial y}=-\frac{1}{\rho_0}\frac{\partial p}{\partial y}+\nu\nabla^2 v+g\alpha(T-T_0), \tag{2}$$

$$\frac{\partial u}{\partial x}+\frac{\partial v}{\partial y}=0, \tag{3}$$

$$\frac{\partial T}{\partial t}+u\frac{\partial T}{\partial x}+v\frac{\partial T}{\partial y}=\kappa\nabla^2 T+Q(x,y,t), \tag{4}$$

where u and v are the horizontal and vertical components of velocity, T the temperature, p the pressure (incorporating the hydrostatic pressure), g the acceleration due to gravity, and ν, ρ_0, α and κ are the kinematic viscosity, density, coefficient of thermal expansion, and thermal diffusivity of the fluid at temperature T_0. The source term $Q(x, y, t)$ corresponds to the rate of temperature increase specified at position

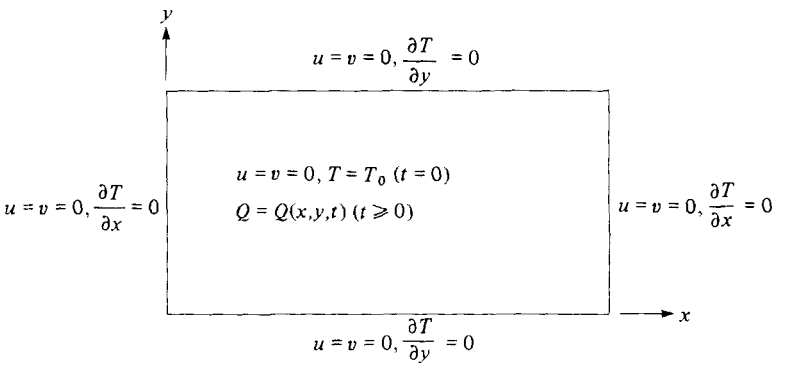

FIGURE 1. The rectangular-cavity notation, boundary and initial conditions.

(x, y) at time t, and in this paper is given the simple form

$$Q(x, y, t) = 2Q_0 h(x - \tfrac{1}{2}L),$$

where Q_0 is a constant with units $°C\ m^{-2}\ s^{-1}$. This form corresponds to a linear horizontal distribution of temperature variation, uniform over the height and in time. The initial and boundary conditions applicable are shown in figure 1.

A scale analysis is now applied to the set (1)–(4) to determine first the appropriate time and velocity scales for the initial core motion, secondly the interaction of the vertical boundaries with the core flow, and thirdly the overall development of the flow to steady state.

2.1. *The core motion*

The motion in the core is, at least initially, driven internally, with the boundaries being regions of adjustment of the temperature and velocity fields; the appropriate horizontal lengthscale is then L, and the vertical scale h.

An examination of the relative magnitudes of the terms of the energy equation (4) yields an initial balance between the unsteady term and the source, provided that $t < t_c$ and $t < t_\kappa$, where, for the current velocity scale u,

$$t_c \sim \frac{L}{u}, \quad t_\kappa \sim \frac{L^2}{\kappa} \tag{5}$$

are the respective timescales for convection and horizontal conduction to dominate the unsteady term. This balance yields a scale for the growth of the temperature difference across the cavity

$$\Delta T \sim Q_0 hLt. \tag{6}$$

The effect of the horizontal temperature gradient is to establish a pressure field which drives a circulation; a balance between the pressure gradient and buoyancy terms in (2) yields a scale for the horizontal pressure gradient

$$\frac{\Delta p}{L} \sim \rho_0 g\alpha Q_0 h^2 t, \tag{7}$$

which, when applied in (1), gives a horizontal velocity scale

$$u \sim \frac{Gr\,\nu^3 t^2}{h^2 L^3}, \tag{8}$$

provided that $t < t_\nu$, $t < t_I$, where

$$t_\nu \sim \frac{h^2}{\nu}, \quad t_I \sim \frac{L}{u} \tag{9}$$

are the respective timescales for the viscous and advection terms to become important. In (8) the effective Grashof number Gr has been introduced:

$$Gr = \frac{g\alpha Q_0 h^4 L^3}{\nu^3}.$$

This definition of Gr is consistent with the usual form if the timescale in (6) is taken as L^2/ν.

The scale (8) holds for $t < t_\nu$, t_κ, t_I and t_c; for $\sigma = \nu/\kappa > 1$, $t_\nu < t_\kappa$, and $t_c \sim t_I$. The relative ordering of t_ν, t_I and t_κ then determines the subsequent flow description. Using (8), $t_I/t_\nu \sim (Gr\,A^4)^{-\frac{1}{3}}$, and the value of Gr relative to A^{-4} then determines the first flow transition.

Consider the case $Gr < A^{-4}$, for which $t_\nu < t_I$. Since $t_c \sim t_I$, (8) holds until $t \sim t_\nu$, when (1) becomes a viscous–pressure-gradient balance, yielding

$$u \sim \frac{Gr\,\nu^2 t}{L^3}. \tag{10}$$

This scale holds if the original energy balance remains unchanged ($t < t_c, t_\kappa$), and advection remains unimportant ($t < t_I$), where t_c is now obtained from (5), and t_I from a balance between the advection and viscous terms, in both cases using (10) as the velocity scale. For $Gr < A^{-4}$, $t_c/t_I < 1$ and the energy balance must switch before the momentum balance. However, from (10)

$$t_c \sim \frac{L^2}{Gr^{\frac{1}{2}}\nu}, \tag{11}$$

and $t_c/t_\kappa \sim Gr^{-\frac{1}{2}}\sigma^{-1}$. Two cases are therefore possible, depending on the relative values of Gr and σ^{-2}. For $Gr < \sigma^{-2}$, $t_\kappa < t_c$, implying that horizontal conduction balances the heat input before convection acts. This suggests that $Gr < \sigma^{-2}$ is a purely conductive regime, with the resulting horizontal gradient driving a weak circulation with a velocity scale

$$u \sim Gr\,\sigma\frac{\nu}{L}. \tag{12}$$

If, however, $Gr > \sigma^{-2}$, $t_c < t_\kappa$, and convection enters the energy balance at t_c, yielding a temperature difference

$$\Delta T \sim \frac{Q_0 h L^2}{u}. \tag{13}$$

The resulting viscous–pressure balance in (1) gives

$$u \sim \frac{Gr\,\nu^2 t}{L^3}, \tag{14}$$

and steady state has been achieved, with t_c being an estimate for the steady-state time.

Both horizontal conduction and convection have small influence on the change in temperature for times less than t_c or t_κ; however, they must provide the heat transport necessary for the system to approach steady state. For small time (and low velocities),

conduction is the transfer mechanism, and remains so if $Gr < \sigma^{-2}$. If $Gr > \sigma^{-2}$, however, convection must, at some time t_{CH}, become the dominant transfer mechanism, where the scale for t_{CH} will depend on one of the velocity scales (8) or (10). Using these scales it may be shown that

$$t_{CH} \sim \frac{hL\kappa^{\frac{1}{2}}}{Gr^{\frac{1}{2}}\nu^{\frac{3}{2}}} \quad \left(Gr > \frac{1}{\sigma A^2}\right),$$

$$\sim \frac{L^2\kappa}{Gr\,\nu^2} \quad \left(Gr < \frac{1}{\sigma A^2}\right). \tag{15}$$

This yields a further division in the flow description at $Gr \sim \sigma^{-1}A^{-2}$; the division, however, determines only the time at which convection becomes important as the horizontal transfer mechanism.

Given that convection begins to act at time t_{CH}, an increasing tendency for the isotherms to become horizontal will become evident. Horizontal isotherms imply a vertical conductive heat transport, which, if it exceeds the horizontal convective transport, will destroy the convective effect. Since the vertical transport is $O(\kappa\,\Delta T/h^2)$, these two effects balance at t_{CV}, where from (8) and (10),

$$t_{CV} \sim \frac{L^2\kappa^{\frac{1}{2}}}{Gr^{\frac{1}{2}}\nu^{\frac{3}{2}}} \quad \left(\frac{1}{\sigma A^4} < Gr\right),$$

$$\sim \frac{L^4\kappa}{Gr\,\nu^2 h^2} \quad \left(\frac{1}{\sigma^2 A^4} < Gr < \frac{1}{\sigma A^4}\right), \tag{16}$$

where two further flow divisions have been obtained, and, for $Gr < \sigma^{-2}A^{-4}$, horizontal convection is unable to exceed the draining effect of vertical conduction. Thus this latter division, $Gr \sim \sigma^{-2}A^{-4}$, gives a lower bound for which convection may be evident.

A similar scaling analysis may be applied for the case $Gr > A^{-4}$. In this case the first change in flow character occurs at $t \sim t_I$; since $t_I \sim t_c$ in this regime, t_I also corresponds to steady state. From (8) and (9)

$$t_I \sim \frac{L^{\frac{4}{3}}h^{\frac{2}{3}}}{Gr^{\frac{1}{3}}\nu}. \tag{17}$$

For $t < t_I$ the velocity scale is given by (8); for $t > t_I$ both thermal and momentum balances change to give

$$u \sim \frac{Gr^{\frac{1}{3}}\nu}{h^{\frac{2}{3}}L^{\frac{1}{3}}}. \tag{18}$$

The secondary timescales t_{CH} and t_{CV} may also be obtained in the same way, giving

$$t_{CH} \sim \frac{hL}{Gr^{\frac{1}{2}}\sigma^{\frac{1}{2}}\nu}, \quad t_{CV} \sim \frac{L^2}{Gr^{\frac{1}{2}}\sigma^{\frac{1}{2}}\nu}, \tag{19}$$

with no further divisions in flow characteristics.

In summary, the time and velocity scales in the core depend on the values of Gr relative to A^{-4}, $\sigma^{-2}A^{-4}$ and σ^{-2}, with secondary divisions at $Gr \sim \sigma^{-1}A^{-4}$, $\sigma^{-1}A^{-2}$. Following consideration of the vertical boundary region, these and other scales will be summarized to give an overall picture of the evolution to steady state.

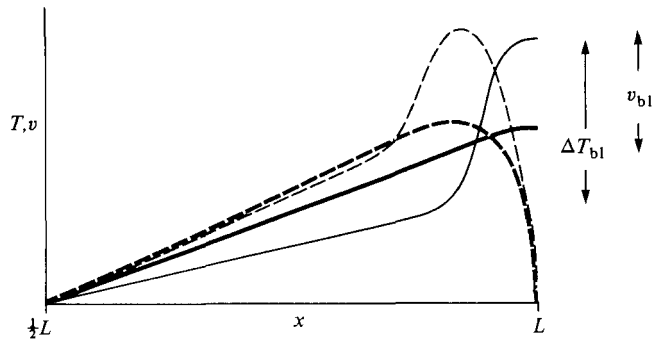

FIGURE 2. An illustration of the adjustments to the temperature and vertical velocity profiles near the wall at the hot end of the cavity. The solid lines are temperature and the broken lines velocity at $t < t_c$ (heavy) and at steady state (light).

2.2. *Adjustments at the vertical boundaries*

As as result of the symmetry of the problem posed, it suffices to consider only the adjustments at the wall of the heated end of the cavity. The temperature adjustment near this wall occurs over a lengthscale $\delta_T \sim \kappa^{\frac{1}{2}}t^{\frac{1}{2}}$. The net rate of heat input to this region of adjustment is $O(Q_0 hLh\delta_T)$, and the rate of conduction away is then $O(\kappa \Delta T h/L)$; this is less than the input for $t < t_\kappa$.

The wall temperature therefore continues to grow until convection becomes important as a core heat-transfer mechanism at $t \sim t_{CV}$. For $t > t_{CV}$, increasing convection in the core results in a reduction in the rate of growth of the horizontal temperature gradient. Near the vertical wall, however, the no-slip condition requires that the core velocity falls away to zero in a region δ_ν, determined by an advection–diffusion of vorticity balance, $\nu^2/h \sim \nu v/\delta_\nu^2$. The velocity reduction results in a reduction in vertical convection of heat away; the region of reduced convection is also the region of maximum heat input because of the form of the source distribution. Since convection in the core has not yet balanced the core heat input, reduced convection in the adjustment region cannot balance the maximum heat input, and conduction away through the core is insufficient to remove the excess heat. The result is a continuing increase in temperature at the wall, at a faster rate than the increase in the core. This increasing temperature must adjust over δ_T to meet the condition $\partial T/\partial x = 0$; since $\delta_T < \delta_\nu$, a steep temperature gradient is set up at δ_ν, which in turn drives an additional flow in an attempt to provide sufficient convection for thermal equilibrium to be achieved near the wall.

The situation is illustrated conceptually in figure 2. The heavy solid and broken lines represent the temperature and vertical velocity profiles as functions of horizontal position at some time $t < t_c$, and the light lines the profiles when equilibrium is achieved. The resulting temperature gradient is sufficient to drive additional convection to balance the heat input over δ_T.

At steady state, conduction over δ_T must balance the heat input,

$$\kappa \Delta T_{bl}/\delta_T \sim Q_0 hL\delta_T,$$

where ΔT_{bl} is the local temperature increase and the excess vertical velocity v_{bl} is obtained from a balance between the viscous and buoyancy forces (Patterson & Imberger 1980), $\nu v_{bl}/\delta_T^2 \sim g\alpha \Delta T_{bl}$. Finally, the excess heat must be convected away

by $v_{\rm bl}$ so that $v_{\rm bl}\,\Delta T_{\rm bl}/h \sim Q_0 hL\delta_\nu$. The result of these three balances is

$$\delta_T \sim \frac{h^{\frac{2}{3}}L^{\frac{1}{3}}}{Gr^{\frac{1}{6}}\sigma^{\frac{1}{3}}}, \quad v_{\rm bl} \sim \frac{\kappa Gr^{\frac{1}{3}}\sigma^{\frac{2}{3}}}{h^{\frac{1}{3}}L^{\frac{2}{3}}}, \quad \Delta T_{\rm bl} \sim Q_0 hL\frac{h^{\frac{1}{3}}L^{\frac{2}{3}}}{Gr^{\frac{1}{3}}\sigma^{\frac{2}{3}}K}, \tag{20}$$

and the timescale for δ_T to reach the value (20) is given by

$$t_{\rm bl} \sim \frac{h^{\frac{4}{3}}L^{\frac{2}{3}}}{Gr^{\frac{1}{6}}\sigma^{\frac{1}{3}}K}, \tag{21}$$

which represents the time for thermal equilibrium near the wall to be achieved.

The scales (20), (21) are based on the assumption that δ_ν, $\delta_T < h$. For $Gr < A^{-4}$ it is easy to show that $\delta_\nu > h$ and the analysis is not valid. The interpretation here is that the adjustment occurs over the scale of the cavity and the core motion is large compared with the boundary adjustment.

On the other hand, if $Gr > A^{-4}$, $v \sim h^{\frac{1}{3}}\nu Gr^{\frac{1}{3}}L^{-\frac{4}{3}}$ from (8) and (17) and

$$\delta_\nu \sim \frac{h^{\frac{1}{3}}L^{\frac{2}{3}}}{Gr^{\frac{1}{6}}}, \tag{22}$$

where now $\delta_\nu < h$. In this case, the vertical layers are distinct, and the boundary influence will be evident.

The motion cannot achieve steady state until the boundary adjustment has stabilized at time $t_{\rm bl}$. For $Gr > A^{-4}$, $t_{\rm bl} > t_{\rm c}$, and the estimate of the steady-state time is extended to $t_{\rm bl}$. For $Gr < A^{-4}$ the effect is dominated by the core motion and will be only weakly, if at all, present. In this case, $t_{\rm bl}$ is an upper estimate of the steady-state time for those Gr-values for which $t_{\rm bl} > t_{\rm c}$; that is, for $Gr > \sigma^{-2}A^{-4}$. For $Gr < \sigma^{-2}A^{-4}$, $t_{\rm c} > t_{\rm bl}$, and $t_{\rm c}$ remains as the steady-state estimate.

A discussion of the interaction between the boundary and core flows is also necessary. This interaction is extremely complex and a detailed scaling analysis is not possible. A qualitative picture of the interaction may, however, be built up. At time $t_{\rm c}$ (with $Gr > A^{-4}$) the core flow has achieved thermal equilibrium; however, since $t_{\rm c} < t_{\rm bl}$, the boundary flow is still accelerating, with a velocity higher than the core. Diffusion of vertical momentum from the boundary region into the core will increase the vertical core velocity beyond its thermal-equilibrium value, with the result that the convective heat transport will now exceed the heat input to the core. The core temperature near the boundary will be reduced, as will the horizontal temperature gradient in the core. On the other hand, the temperature gradient at the edge of the boundary region is increased. Consequently, the forcing for the core motion is reduced and the forcing for the boundary motion is increased.

The result of these adjustments is then a reduction in the horizontal core temperature gradient at the expense of an increased wall gradient. As the boundary velocity increases, an increasing section of the core is driven by diffusion of momentum from the boundary, further decreasing the core gradient. Should the core gradient become negative, the core forcing becomes negative, increasing the shear between core and boundary, and tending to reduce the boundary motion. This two-way interaction provides a mechanism for the generation of internal waves, which represent the adjustment of the flow and temperature fields in the core region influenced by diffusion of momentum from the boundary region into the core. At steady state, this region of the core will be driven entirely by this diffusion of momentum, the flow being just sufficient to balance the heat input, and the isotherms will be horizontal. For large Grashof numbers, the region will encompass the entire core. Thus, in the

Timescale	Parameter, equation	Comments
		Regime: $\sigma^4 A^{-4} < Gr$
$Gr^{-\frac{1}{2}}\sigma^{-\frac{1}{2}}A^{-1}$	t^*_{CH} (19)	Pure-conduction phase complete as convection becomes important. Vertical conduction dismantles vertical structure. Core velocity scale given by (11), boundary scales by (32).
$Gr^{-\frac{1}{2}}\sigma^{-\frac{1}{2}}A^{-2}$	t^*_{CV} (19)	Convection dominates heat transfer, and significant deviation from pure conduction begins.
$Gr^{-\frac{1}{3}}A^{-\frac{4}{3}}$	t^*_c, t^*_I (17)	Thermal balance in the core, but boundary adjustment continues. Sharp gradients near the vertical walls, and Nu approaches a maximum as internal-wave activity begins.
$Gr^{-\frac{1}{6}}\sigma^{\frac{2}{3}}A^{-\frac{2}{3}}$	t^*_{bl} (21)	Boundary adjustment complete. Internal-wave activity continues.
1	t^*_ν (9)	Steady state as internal wave activity decays.
		Regime: $A^{-4} < Gr < \sigma^4 A^{-4}$
$Gr^{-\frac{1}{3}}A^{-\frac{4}{3}}$	t^*_c, t^*_I (17)	Flow development as above.
1	t^*_ν (9)	Internal-wave activity decayed, boundary adjustment continues, and smooth approach to steady state begins.
$Gr^{-\frac{1}{6}}\sigma^{\frac{2}{3}}A^{-\frac{2}{3}}$	t^*_{bl} (21)	Steady state as boundary adjustments complete.
		Regime: $\sigma^{-1}A^{-4} < Gr < A^{-4}$
$Gr^{-\frac{1}{2}}\sigma^{-\frac{1}{2}}A^{-2}$	t^*_{CV} (16)	Flow development as above.
1	t^*_ν (9)	Core flow scaling becomes viscous (19).
$Gr^{-\frac{1}{2}}A^{-2}$	t^*_c (11)	Thermal balance in the core, but boundary adjustment continues. Scale of boundary adjustments is $O(h)$ and effect is weak. Weak internal waves may be present, heavily damped.
$Gr^{-\frac{1}{6}}\sigma^{\frac{2}{3}}A^{-\frac{2}{3}}$	t^*_{bl} (21)	Boundary-layer adjustment complete. Steady state achieved by steady approach. t^*_{bl} is an upper estimate of steady-state time.
		Regime: $\sigma^{-2}A^{-4} < Gr < \sigma^{-1}A^{-4}$
$Gr^{-\frac{1}{2}}\sigma^{-\frac{1}{2}}A^{-1}$	t^*_{CH} (15)	Flow development as above.
1	t^*_ν (9)	Flow switches to viscous domination (19). Heat transfer by augmented conduction.
$Gr^{-1}\sigma^{-1}A^{-4}$	t^*_{CV} (16)	Convection dominates vertical conduction, and significant deviation from the pure conduction solution begins.
$Gr^{-\frac{1}{2}}A^{-2}$	t^*_c (11)	Thermal balance in the core. Weak-internal-wave activity and evidence of boundary adjustment.
$Gr^{-\frac{1}{6}}\sigma^{\frac{2}{3}}A^{-\frac{2}{3}}$	t^*_{bl} (21)	Boundary-layer adjustment complete.
		Regime: $\sigma^{-1}A^{-2} < Gr < \sigma^{-2}A^{-4}$
1	t^*_ν (9)	Flow development as in previous case.
$Gr^{-\frac{1}{2}}A^{-2} \to \sigma A^{-2}$	t^*_c (11) $\downarrow$ t^*_κ (15)	Steady state by augmented conduction. No boundary effects.

Timescale	Parameter, equation	Comments
		Regime: $\sigma^{-2} < Gr < \sigma^{-1}A^{-2}$
$Gr^{-1}\sigma^{-1}A^{-2}$	t^*_{CH} (15)	Augmented conduction begins.
$Gr^{-\frac{1}{3}}A^{-2} \to \sigma A^{-2}$	t^*_c (11) $\downarrow$ t^*_κ (5)	Steady state by augmented conduction.
		Regime: $Gr < \sigma^{-2}$
σA^{-2}	t^*_κ (5)	Pure conduction.

TABLE 1

convective limit at steady state the entire flow is driven by the boundary flow, as in the differentially heated endwall case, although completely different mechanisms are responsible and the scales are different.

2.3. *Internal-wave activity*

The possibility of internal waves generated by the mechanism described above implies a delayed timescale for the achievement of steady state. An upper estimate for the decay time of these waves is $t_\nu \sim h^2/\nu$. The internal waves will have frequency $O(\omega)$, where, from Fischer *et al.* (1979),

$$\omega \sim \frac{N}{(1+A^{-2})^{\frac{1}{2}}} \sim NA \quad (A < 1), \tag{23}$$

with the Brunt–Väisälä frequency, based on the mean vertical temperature gradient at t_c, given by $N \sim Gr^{\frac{1}{3}}\nu/h^{\frac{5}{3}}L^{\frac{1}{3}}$, for $Gr > A^{-4}$. The period of oscillation is then $O(t_N)$,

$$t_N \sim \frac{h^{\frac{5}{3}}L^{\frac{1}{3}}}{Gr^{\frac{1}{3}}\nu A}, \tag{24}$$

and, since $t_N < t_\nu$ for $Gr > A^{-4}$, the wave activity will be present and steady state will be achieved in a decaying oscillatory fashion. The previous estimate of steady-state time for $Gr > A^{-4}$ was t_{bl}; the two estimates balance at $Gr \sim \sigma^4 A^{-4}$. Thus for $Gr < \sigma^4 A^{-4}$, $t_{bl} > t_\nu$, and the waves have decayed before steady state is achieved. On the other hand, if $Gr > \sigma^4 A^{-4}$, the vertical adjustment region is stabilized before the wave motion has died away. In the first case the final approach to steady state is smooth, in the second it is oscillatory.

2.4. *Overall evolution to steady state*

The results of §§2.1–2.3 may be summarized to form an overall picture of the development of the flow from initiation to steady state for a particular set of parameter values. The six Grashof-number criteria noted above divide the Grashof-number space into a number of transient flow regimes, each of which is characterized by a different approach to steady state. Some of these differences are slight, and a broader classification into three regimes is possible: conductive ($Gr < \sigma^{-2}$), augmented conductive or transitional ($\sigma^{-2} < Gr < \sigma^{-2}A^{-4}$), and convective ($Gr > \sigma^{-2}A^{-4}$). The first of these regimes is characterized by the complete absence of convective effects, and the third by their dominance and an oscillatory approach to steady state. The

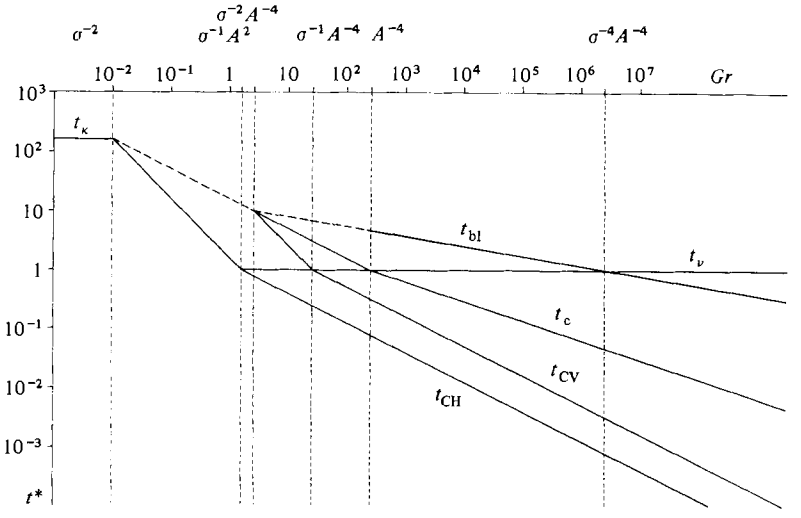

FIGURE 3. The variation with Gr of the various timescales in their regions of validity for the case $\sigma = 10$, $A = 0.25$. The broken vertical lines represent regime boundaries.

transitional regime lies between these extremes, its characteristics depending on the location of Gr within the regime.

The remaining parameters define a number of subregimes of the broader classification. For $\sigma > 1$, $A < 1$, two orderings of the Grashof-number criteria are possible, depending on the value of σA^2. In the following it is assumed that $\sigma A^2 < 1$, giving

$$\frac{\sigma^4}{A^4} > \frac{1}{A^4} > \frac{1}{\sigma A^4} > \frac{1}{\sigma^2 A^4} > \frac{1}{\sigma A^2} > \frac{1}{\sigma^2}.$$

The evolution to steady state in each of the seven regimes is summarized by table 1, which briefly describes the hierarchy of timescales that divide each regime into a number of transient flow subregimes, and by figure 3, which, for particular values $\sigma = 10$, $A = 0.25$, shows the variation of Gr of the relevant timescales (non-dimensionalized by $h^2\nu^{-1}$) in each regime.

3. Numerical procedures, results and discussion

To test the validity of the scale analysis and interpretation of §2, numerical solutions for the case $\sigma = 10$, $A = 0.25$ have been obtained for various values of Gr, the Gr-values being selected to allow access to as many as possible of the regimes. All computations were carried out on square, uniformly spaced grids, using the algorithm described by Patterson & Imberger (1980), with appropriate modifications to the energy equation and boundary conditions. Further discussion of the algorithm is not warranted here, except to note that increasing difficulty in converging to a final Nusselt number of unity (as required by the insulated-wall boundary conditions) with increasing Grashof number severely limited the maximum Grashof number for which computations could be carried out.

Before differencing, (1)–(4) were non-dimensionalized according to the scheme

$$X = \frac{x}{h}, \quad Y = \frac{y}{h}, \quad t^* = \frac{t\nu}{h^2}, \quad U = \frac{uh}{\nu}, \quad V = \frac{vh}{\nu}, \quad T^* = \frac{(T-T_0)\kappa}{Q_0 hL^3}, \quad P = \frac{ph^2}{\rho_0 \nu^2},$$

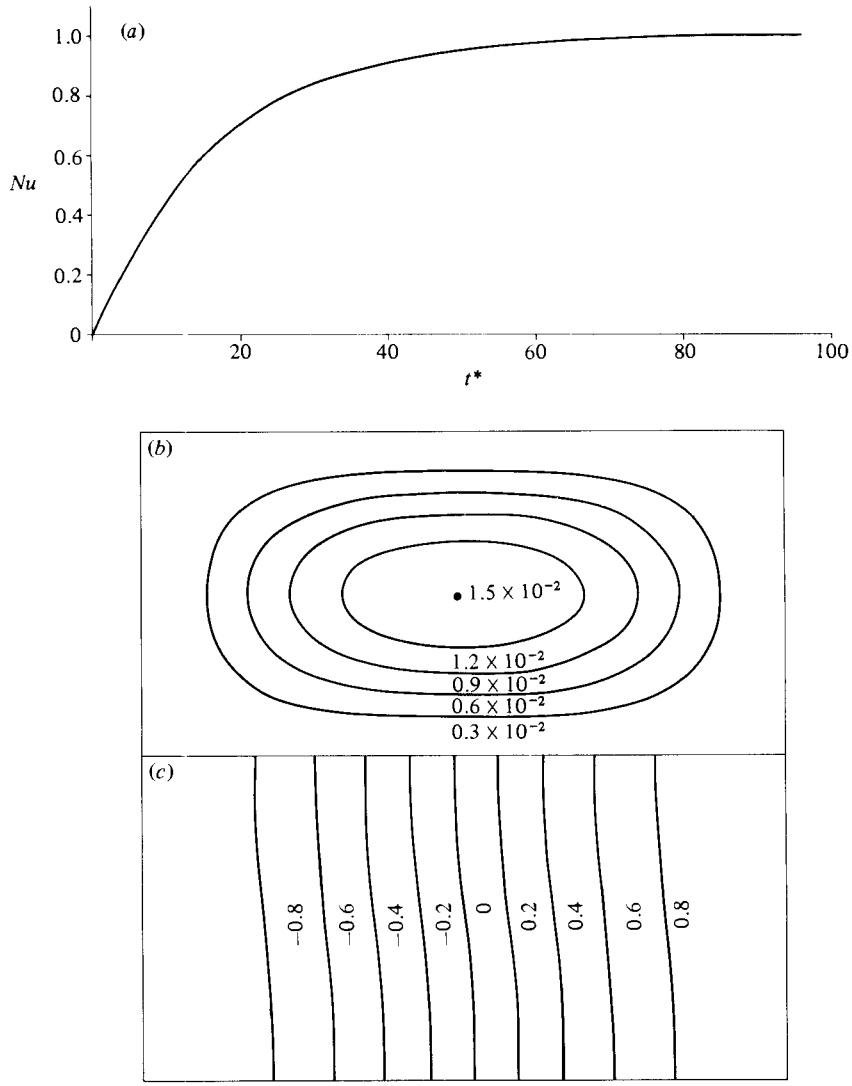

FIGURE 4. The numerical results for run 1, $Gr = 0.625$: (*a*) the variation of Nu with t^*; (*b*) the steady-state streamlines; (*c*) the steady-state isotherms. T^* has been normalized by $T^*_{\max}$, and the numerical values in (*b*) are values of ϕ/ν.

and the transport equations were written in conservative form. In terms of the non-dimensional variables, the Nusselt number at the centreline of the cavity is given by

$$Nu = -\frac{2}{A}\int_0^2 \left(\sigma U T^* - \frac{\partial T^*}{\partial X}\right)_{X=1/2A} \mathrm{d}Y.$$

The variation of Nu with non-dimensional time gives an indication of the effect of convection as its value deviates from the pure conduction result, evidence of the presence of internal-wave activity, and a measure of the progress of the integration. When the computed value of Nu differs from unity by less than a prescribed amount for a sufficient time, steady state is assumed to have been achieved, after confirmation

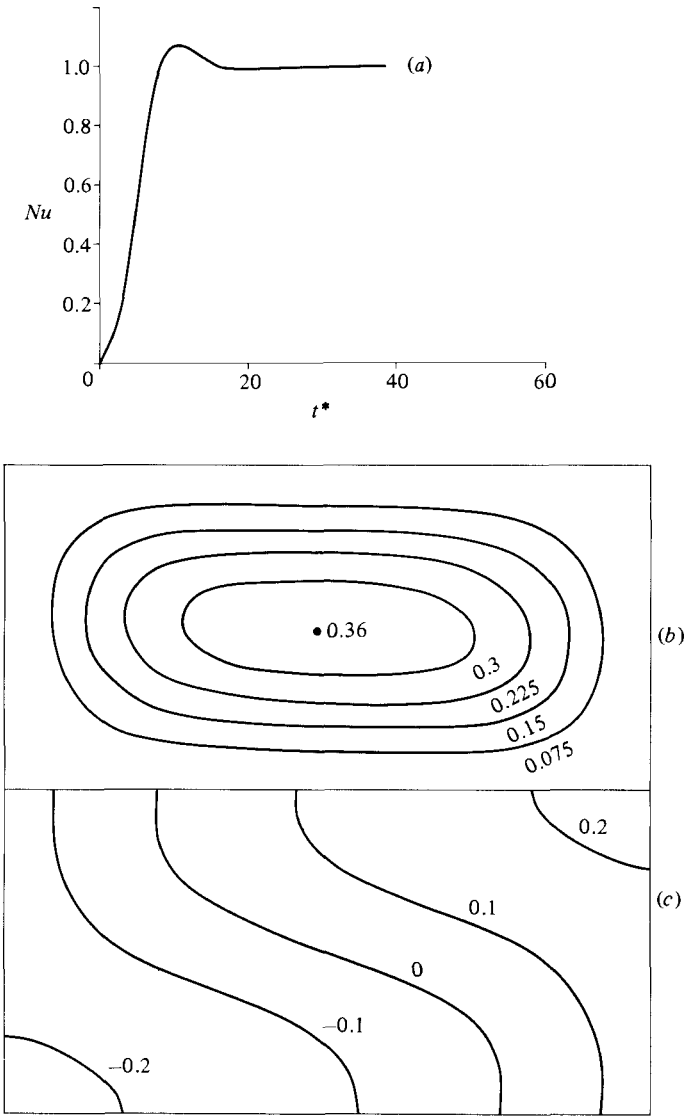

FIGURE 5(*a–c*). For caption see facing page.

by the iteration count. The asymptotic approach to steady state, however, implies a large potential error in the numerical estimate of steady-state time.

The pure conduction solution may be obtained by the usual transform methods as

$$T(x,y,t) = T_0 - \frac{8hL^3Q_0}{\kappa\pi^4} \sum_{m=1}^{\infty} \frac{1-e^{-\kappa(2m-1)^2\pi^2 t/L^2}}{(2m-1)^4} \cos\frac{(2m-1)\pi x}{L}.$$

At steady state, this becomes, in non-dimensional form,

$$T^* = -2(\tfrac{1}{6}X^3A^3 - \tfrac{1}{4}X^2A^2 + \tfrac{1}{24}),$$

which has maximum magnitude of $T^*_{\max} = 0.0833$ at either endwall. As convection becomes important, the maximum non-dimensional temperature is reduced. In the results given below, the temperatures have been normalized by $T^*_{\max}$.

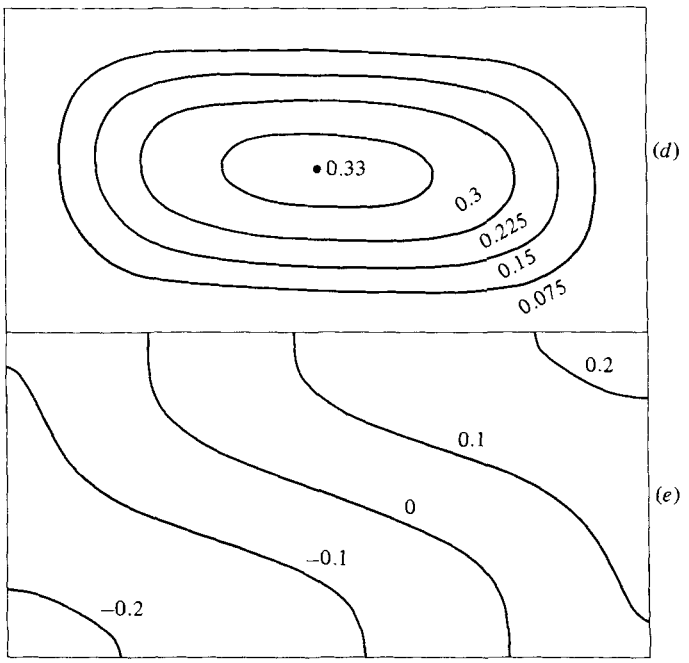

FIGURE 5. The numerical results for run 2, $Gr = 62.5$: (*a*) the variation of Nu with t^*; (*b*), (*c*) the flow and temperature fields at the peak in (*a*), $t^* = 10$; (*d*), (*e*) the flow and temperature fields at steady state. T^* has been normalized by $T^*_{\max}$, and the numerical values in (*b*) and (*d*) are values of ϕ/ν. Note the change in timescale.

The computations have been carried out for $\sigma = 10$, $A = 0.25$, with Gr ranging between 0.625 and 6.25×10^4, traversing all regimes except $Gr < \sigma^{-2}$ and $Gr > \sigma^4 A^{-4}$. The region $Gr < \sigma^{-2}$ was not included as little would be learned by the solution of essentially a pure-conduction problem. The region $Gr > \sigma^4 A^{-4}$ was beyond the limit of economical computation and was excluded as the $Gr \sim 6.25 \times 10^4$ case would display many of the features of this region. The computations shown in figures 4–6 were for Gr-values of 0.625, 62.5 and 6.25×10^4. Other values, representative of the remaining regimes, were also used; these showed a transition between the values above and the results are not shown. In each of the figures the variation of Nu with t^* is shown, indicating the progression to steady state, the influence of convection and the presence or otherwise of internal-wave activity. The flow and temperature (normalized by $T^*_{\max}$) fields at steady state are also shown, and in some cases the fields at some time before steady state are given as well.

The first computation (figure 4, $Gr = 0.625$) lies in the transitional regime and shows a monotonic approach to steady state. The steady flow field shows a weak circulation which has a minor convective effect on the temperature field, which is dominated by conduction. With increasing Gr, this convective influence increases; figure 5 shows the results for $Gr = 62.5$, in the convective regime $\sigma^{-2}A^{-4} < Gr < A^{-4}$, close to the upper boundary where adjustments at the vertical boundary become important. The Nusselt number shows a rapid rise to a value greater than unity, followed by a slow decay away to unity, indicating the dominance of convection and the presence of heavily damped internal wave activity. The flow and temperature fields at the maximum Nu-value ($t^* = 10$) are shown in figures 5(*b*, *c*), and the steady-state fields in figures 5(*d*, *e*). Both the velocities and horizontal temperature gradient are less at

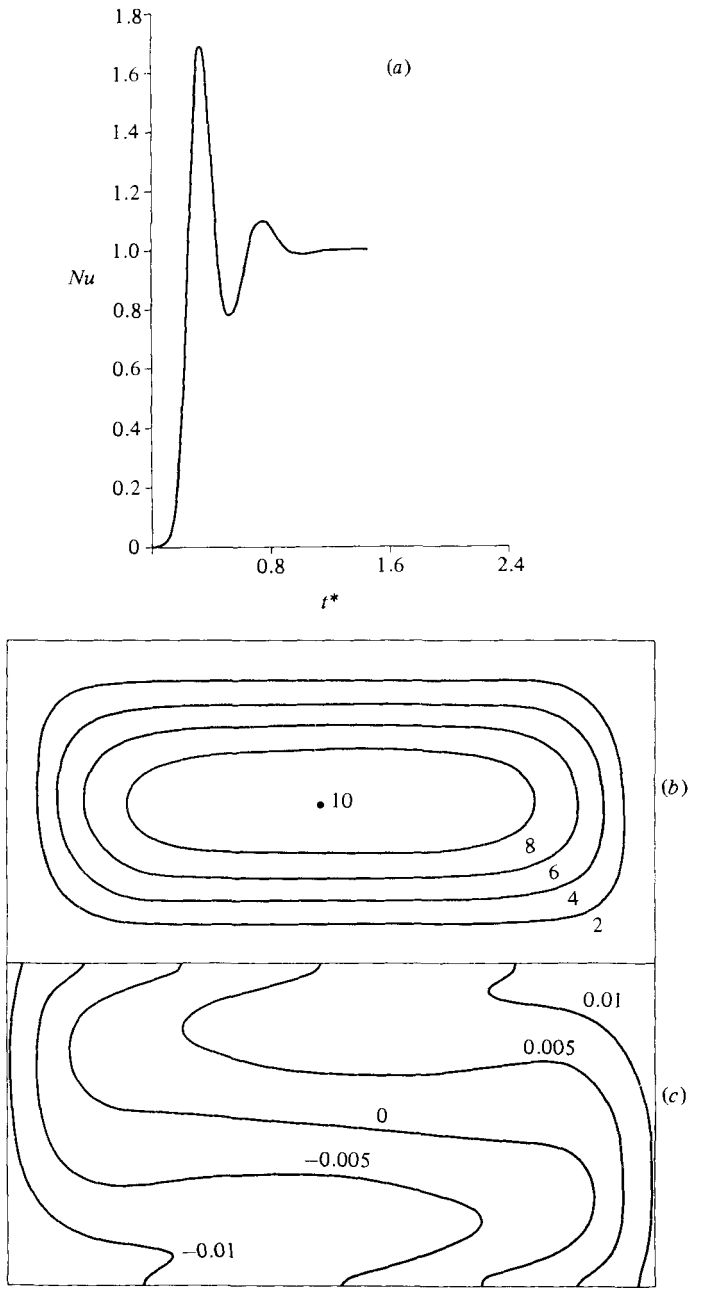

FIGURE 6(*a–c*). For caption see facing page.

steady state as a result of the decaying internal wave. The isotherms have gone through significant adjustment near the vertical boundaries, an indication that, although $Gr < A^{-4}$, the vertical-wall adjustments are beginning to have some effect. The maximum temperature is reduced to a normalized value of 0.22; evidently horizontal conduction is playing a very little role in the heat-transfer process.

The final computation shown is for $Gr = 6.25 \times 10^4$, for which $Gr > A^{-4}$. Convection and adjustments near the vertical boundaries are expected, and internal-wave

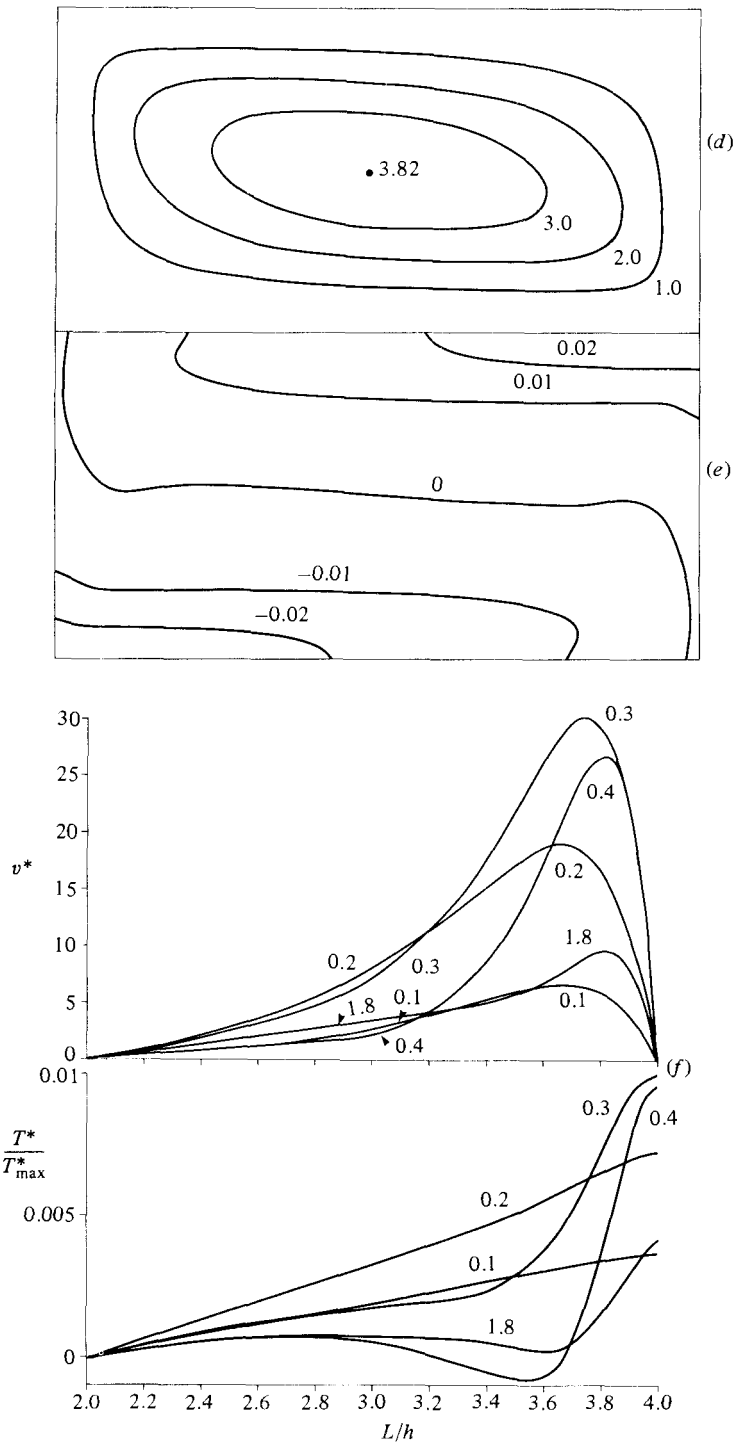

FIGURE 6. The numerical results from run 3, $Gr = 6.25 \times 10^4$: (*a*) the variation of Nu with t^*; (*b*), (*c*) the flow and temperature fields at the first peak in (*a*), $t^* = 0.33$; (*d*), (*e*) the flow and temperature fields at steady state; (*f*) the development of the mid-depth vertical-velocity and temperature profiles in the heated end of the cavity as functions of time. T^* has been normalized by $T^*_{\max}$, and the numerical values in (*b*) and (*d*) are values of ϕ/ν. The numerical values in (*f*) are the values of t^* at which the profiles of V and T^* are taken.

activity is likely, and, since Gr is close to the boundary of the inertial regime, inertial effects will be present. The Nusselt number (figure 6a) shows internal wave activity of period 0.41 (compared with 0.16, from (24)) decaying to unity. This mismatch of periods indicates that the details of the vertical stratification may be important in (24). However, the periods are of the same order. The flow and temperature fields at the peak Nu-value (figures 6b, c) and steady state (figures 6d, c) show evidence of inertial intrusions travelling across the cavity on a scale less than h, large temperature gradients and velocity concentrations near the vertical boundaries, and significant adjustments near these boundaries as steady state is reached. At steady state, the core flow is driven almost entirely by diffusion of momentum from the velocity concentrations near the vertical walls; in turn, the velocity concentration is generated by the steep temperature gradient.

The development of the adjustments near the vertical boundaries is better shown by figure 6(f), which depicts the vertical velocity and temperature profiles at the mid-depth of the cavity as a function of x, for the heated half of the cavity, as time progresses. This shows that the increasing linear core temperature gradient generates a vertical velocity, tending to concentrate near the boundary. By $t^* = 0.3$, diffusion of momentum from the concentration has been sufficient to reduce the core gradient, and by $t^* = 0.4$, the gradient has become negative, reducing the velocity peak. This reversal began at $t^* = 0.33$, corresponding to the peak Nu-value. These adjustments continue until at steady state, $t^* = 1.8$, the core temperature is essentially uniform. Near the boundary, the temperature gradient drives a flow which is sufficient to achieve thermal equilibrium in the boundary region, as well as, by diffusion of momentum, in the core region.

4. Conclusions

The results above indicate that convective flows driven by internal buoyancy sources and sinks distributed throughout the cavity may be classified as conductive, transitional or convective, depending on the value of the Grashof number Gr relative to various combinations of the Prandtl number σ and the aspect ratio A. This is a similar conclusion to that reached in Patterson & Imberger (1980) for the differentially heated endwall case. In fact, the flows in each region are qualitatively similar in both cases, with the low Grashof number (low Rayleigh number for the differentially heated endwalls case) flows being characterized by vertical isotherms and a near-linear gradient driving a weak circulation, and the high-Grashof-(Rayleigh-)number flows being characterized by horizontal isotherms in the core region with sharp temperature and velocity gradients near the vertical walls. The mechanisms and scales however in the two cases are quite different.

This research was completed while the author was on sabbatical leave at the National Water Research Institute, Burlington, Ontario, Canada. Grateful acknowledgement is given for the support provided during this period by Environment Canada and by the Gledden Foundation of The University of Western Australia in the form of a Gledden Overseas Fellowship. Initial support was provided by the Australian Research Grants Committee under Grant F7915301. The author also acknowledges useful discussions held with Drs P. F. Hamblin and G. N. Ivey, and comments on the manuscript by Professor J. Imberger.

REFERENCES

BERGHOLZ, R. F. 1980 *Trans ASME* C: *J. Heat Transfer* **102**, 242.

CORMACK, D. E., LEAL, L. G. & IMBERGER, J. 1974 *J. Fluid Mech.* **65**, 209.

FISCHER, H. B., LIST, E. J., KOH, R. C. Y., IMBERGER, J. & BROOKS, N. H. 1979 *Mixing in Inland and Coastal Waters*. Academic.

KIKUCHI, Y., KAWASAKI, T. & SHIOYAMA, T. 1982 *Intl J. Heat Mass Transfer* **25**, 363.

KULACKI, F. A. & GOLDSTEIN, R. J. 1972 *J. Fluid Mech.* **55**, 271.

PATTERSON, J. & IMBERGER, J. 1980 *J. Fluid Mech.* **100**, 65.

ROBERTS, P. H. 1967 *J. Fluid Mech.* **30**, 33.

THIRLBY, R. 1970 *J. Fluid Mech.* **44**, 673.

TRITTON, D. J. & ZARRAGA, M. N. 1967 *J. Fluid Mech.* **30**, 21.

TURCOTTE, D. L., SPENCE, D. A. & BAU, H. H. 1982 *Intl J. Heat Mass Transfer* **25**, 699.